ISSN: 2476-6909; Modares. Mech. Eng. *2026;26(12):969-976.*

Modares Mechanical Engineering

DOI: 10.48311/mme.2026.118668.82925
journal homepage: mme.modares.ac.ir

Numerical Investigation of Alumina-Oil Nanofluid Immersion Cooling for a Single Lithium Iron Phosphate Battery

Alireza Izanlou[1] Mohammad Hatami[2*]

[1] Department of Mechanical Engineering, Ferdowsi University of Mashhad
[2] Department of Mechanical Engineering, Esfarayen University of Technology (EUT)

ARTICLE INFO

Article Type
Original Research

Article History
Received: January 06, 2026
Revised: April 26, 2026
Accepted: June 13, 2026
ePublished: September 17, 2026

ABSTRACT

Lithium-ion batteries are extensively acknowledged as efficient devices for energy storage due to their capacity to function at elevated power levels while ensuring stability and reliability. Nonetheless, a significant obstacle in their real-world application is the heat generation that occurs during both charging and discharging processes, which can adversely impact performance, safety, and lifespan. Consequently, research into thermal management strategies has become crucial to facilitate the stable functioning of lithium-ion batteries. This study presents a numerical analysis aimed at investigating the cooling effectiveness of an Oil/Al_2O_3 nanofluid when utilized with a single lithium iron phosphate (LFP) battery. The research scrutinized a total of six parameters, including four dependent variables associated with the thermophysical characteristics of the coolant, one parameter related with the electrical current passing through the battery, as well as one independent variable related to the nanoparticle volume fraction. Simulations were conducted utilizing the commercial software ANSYS Fluent, maintaining the flow conditions at a constant Reynolds number. To assess the impact of nanoparticle concentration, pure oil was juxtaposed with Oil/Al_2O_3 nanofluid across three distinct volume fractions. The findings revealed that although an increase in nanoparticle concentration from 0% to 4% substantially improved heat transfer, resulting in approximately a 20% enhancement in both the average convective heat transfer coefficient and the Nusselt number, it significantly increases pressure drop along the battery chamber, which ultimately results in a slight decrease in performance efficiency of nanofluid.

Keywords: Heat Transfer Enhancement, LFP Battery, Immersion Cooling, Nanofluid

How to cite this article
Izanlou A, Hatami M, Numerical Investigation of Alumina-Oil Nanofluid Immersion Cooling for a Single Lithium Iron Phosphate Battery. Modares Mechanical Engineering; *2026;26(12):969-976.*

*Corresponding author's email: m.hatami@esfarayen.ac.ir
*Corresponding ORCID ID: 0000-0001-5657-6445

شاپا: ۷۹۰۹-۲۴۷۶؛ مهندسی مکانیک مدرس. ۹۷۶-۹۷۹:(۱۲)۲۶;۱۴۰۵

مهندسی مکانیک مدرس

DOI: 10.48311/mme.2026.118668.82925

صفحه اصلی مجله: mme.modares.ac.ir

بررسی عددی خنک‌سازی غوطه‌وری نانوسیال آلومینا-روغن برای یک باتری لیتیوم-فسفات آهن

علیرضا ایزانلو[۱]، محمد حاتمی[۲]*

[۱] گروه مهندسی مکانیک، دانشگاه فردوسي مشهد، مشهد، ایران

[۲] گروه مهندسی مکانیک ، مجتمع آموزش عالي فني و مهندسي اسفراین، اسفراین، ایران

اطلاعات مقاله

نوع مقاله

مقاله پژوهشی

تاریخچه مقاله

دریافت: ۱۴۰۴/۱۰/۱۶

بازنگری: ۱۴۰۵/۰۲/۰۶

پذیرش: ۱۴۰۵/۰۳/۲۳

ارائه آنلاین: ۱۴۰۵/۰۶/۲۶

چکیده

باتری‌های لیتیوم-یون به دلیل ظرفیت عملکرد در سطوح توان بالا و در عین حال تضمین پایداری و قابلیت اطمینان، به عنوان دستگاه‌های کارآمد برای ذخیره‌سازی انرژی شناخته می‌شوند. با این وجود، یک مانع مهم در کاربرد واقعی آنها، تولید گرما است که در طول هر دو فرآیند شارژ و دشارژ رخ می‌دهد و می‌تواند بر عملکرد، ایمنی و طول عمر تأثیر منفی بگذارد. در نتیجه، تحقیق در مورد استراتژی‌های مدیریت حرارتی برای تسهیل عملکرد پایدار باتری‌های لیتیوم-یون بسیار مهم شده است. این مطالعه یک تحلیل عددی با هدف بررسی اثربخشی خنک‌سازی یک نانوسیال روغن-آلومینا هنگام استفاده با یک باتری فسفات آهن لیتیوم (LFP) ارائه می‌دهد. این تحقیق در مجموع شش پارامتر، از جمله چهار پارامتر وابسته مرتبط با ویژگی‌های ترموفیزیکی خنک‌کننده، یک پارامتر مرتبط با شدت جریان برق عبوری از باتری و همچنین یک متغیر مستقل مرتبط با کسر حجمی نانوذرات را بررسی کرد. شبیه‌سازی‌ها با استفاده از نرم‌افزار تجاری ANSYS Fluent انجام شد و شرایط جریان در عدد رینولدز ثابت حفظ شد. برای ارزیابی تأثیر غلظت نانوذرات، روغن خالص با نانوسیال روغن-آلومینا در سه کسر حجمی مجزا کنار هم قرار داده شد. یافته‌ها نشان داد که اگرچه افزایش غلظت نانوذرات از ۰٪ به ٤٪، انتقال حرارت را به طور قابل توجهی بهبود می‌بخشد و منجر به افزایش تقریباً ۲۰ درصدی ضریب انتقال حرارت جابجایي و عدد ناسلت می‌شود، با اینحال این افزایش به قیمت افزایش قابل توجه افت فشار در طول محفظه باتری حاصل می شود که نهایتا منجر به کاهش مختصر بازدهی کارآیی نانوسیال می گردد.

کلیدواژه‌ها: بهبود انتقال حرارت، باتري ليتيومي، خنك‌كاري غوطه وري، نانوسیال

نحوه ارجاع به این مقاله

ایزانلو علیرضا، حاتمی محمد، بررسی عددی خنک‌سازی غوطه‌وری نانوسیال آلومینا-روغن برای یک باتری لیتیوم-فسفات آهن، مهندسی مکانیک مدرس. ۹۷۶-۹۷۹:(۱۲)۲۶;۱۴۰۵

*پست الکترونیکی نویسنده عهده‌دار مکاتبات: m.hatami@esfarayen.ac.ir

*شناسه ارکید نویسنده عهده‌دار مکاتبات: 0000-0001-5657-6445

1- Introduction

Energy management has been acknowledged as a fundamental issue in contemporary engineering, considering that energy has traditionally been vital for the survival and advancement of human civilization. Al-Hallaj et al. [1] considered an experimental configuration and came up with a passive cooling system that consists of applying Phase Change Materials (PCMs), and it was demonstrated that under circumstances close to thermal insulation and an air convective coefficient of heat transfer equal to zero, applying PCMs reduced the temperature of a 100 Ah pack by 8°C with respect to cases without PCMs. Liquid cooling offers a highly efficient air substitute for battery thermal systems in electric vehicles at the scale possible for commercial-scale manufacture, given the increased heat capacity of liquids over air and their enhanced thermal conductivity [2]. Experimental and numerical simulation studies on the effect of free convection air cooling on a lithium iron phosphate pouch battery were carried out by Kalkan et al. [3] The results of the study also indicated that free convection air cooling is ineffective for managing high discharges of batteries. Cheng et al. [4] designed and tested a single-phase forced convection immersion cooling system for electronic devices through both numerical simulation and experimental procedures. During this study, the motherboard assembly was immersed in a specially created cooling fluid that was referred to as Novec 7100. The results showed that there is a relation between elevated coolant velocities and the enhanced removal of heat from the processor, which leads to lower processor temperatures; conversely, reduced flow velocities have elevated temperatures and a nonuniform temperature distribution as their consequence. The numerical performance study of immersion cooling of a pouch battery module was carried out by Zhou et al. [5] using ANSYS Fluent and was also compared with air cooling results. The study underscored that the immersion cooling method adopted was effective in balancing the maximum temperature and maximum temperature difference in the battery pack, such that these parameters were very low for a 3C discharge rate for immersion cooling compared with air cooling. Besides that, the cooling efficiency is greatly influenced by the coolant's flow rate in immersion cooling; it will reduce with the increase of this factor but will increase pressure drop, and as such, optimization of this flow rate will be inevitable. Patil et al. [6] proposed a new cooling method for a lithium pouch battery module using numerical simulation and experimental study. In this study, the batteries were submerged in a dynamic cooling medium, and the researchers designed an air duct that is positioned at the upstream side of the module and incorporated the terminals of the batteries, which were the hottest points on the batteries, to increase the circulation of air. The comparison of various cooling setups highlighted that the coolest cooling arrangement is comprised of coolant flow with air in the upstream duct such that the temperature of the terminals of the battery can be lowered by 46.8% as compared to utilizing independent free convection air cooling. Gharehghani et al. [7] numerically simulated a new cooling system utilizing indirect side cooling with the use of aluminum plates. The study entailed the use of two aluminum plates, which were located on either side of the batteries and equipped with six microchannels for water passage. This study examined the effect of different geometries of water microchannels that were divided into four different types, namely straight, wavy, porous, and those with thin metal foam layer coverage on the walls, on cooling efficiency. The results proved that wavy microchannels and those with porous aluminum foam increase significantly the rate of heat transfer and thereby reduce the overall temperature of the battery module on average. Zou et al. [8] numerically analyzed an inline-configured cylindrical 18650 battery module for investigation of the hybrid cooling comprising static immersion cooling with mineral oil and indirect cooling with water-contact tubes located between the battery columns. The approach, in this case, involves the absorption of the collected heat with the oil and the rejection with the flowing water in the tubes. The maximum temperature and temperature difference across the battery module under natural conditions were below 43.3°C and 2.62°C, respectively, as per the results obtained. The system has an advantage over dynamic cooling systems, for instance, in lower energy usage. Ahmad et al. [9] employed a new approach that combines numerical solutions with artificial neural networks to examine the effects of dynamic immersion cooling and determine the best cooling conditions. The study considered parameters such as spacing between batteries, distance from walls, inlet velocity of flows, and the amount of flows within a 10-prismatic-battery-module battery module. The results showed that dynamic immersion cooling produces an 8.3% higher reduction in the maximum temperature of the battery module than static immersion cooling. In addition, the use of neural networks yielded 7.7% and 86% reduction in maximum temperature and temperature difference, respectively, compared with cases without neural networks. Yang et al. [10] performed a computational simulation on a 20-cell lithium iron phosphate battery module to examine the effect of dynamic immersion cooling using supercritical carbon dioxide (S-CO2), which is distinguished by its superior thermophysical properties, such as high heat capacity and superior thermal conductivity compared with conventional immersion cooling liquids. Their results showed that this technique significantly enhances the overall efficiency of thermal management with a 453% increase in the Nusselt number compared with mineral oil as the cooling agent. However, this system poses safety issues and requires high-pressure-capable battery modules. Based on above literature review, presenting a numerical analysis to investigate the cooling effectiveness of an Oil/Al_2O_3 nanofluid in batteries is necessary especially when utilized with a single lithium iron phosphate (LFP) due to their advantages and low costs compared to experimental methods. So, this research is performed by this aim and considered a total of six parameters, including four dependent variables associated with the thermophysical characteristics of the coolant, one parameter related with the electrical current passing through the battery, as well as one independent variable related to the nanoparticle volume fraction.

2- Numerical methods

In the current study, a cylindrical lithium iron phosphate (LFP) battery with a radius of (r = 13.125 mm) and a height of (h = 65.4 mm) was utilized. The battery is encapsulated within a rectangular shell with dimensions expressed as (4r ×h × 8r), as presented in Figure (1). The physical properties of the battery materials are given in Table (1). The simulation was performed in the transient regime, for a time period of 1500 seconds. The heating sources inside the battery consist of two major parts [11]: irreversible heat (Joule heating) and reversible heat (Entropic heating). The first type stems from electrical resistance within the battery, whereas the second stems from chemical reactions inside the battery. Previous studies have indicated that the reversible heat on average represents about 20% of the irreversible heat [11], [12]. Consequently, the modeling of the heating sources inside the battery is given following Equation (1).

$$\dot{Q}_{gen}[W] \sim 1.2 R_i I^2 \quad (1)$$

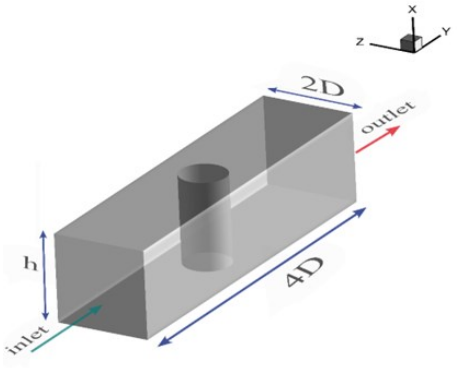

Fig. 1 Schematic of the Geometry

Physical Properties	Value
$C_p\ (\frac{J}{kg.K})$	890
$\rho\ (\frac{kg}{m^3})$	2401.55
$k_{\perp}(\frac{W}{m.K})$	1.26
$k_{\parallel}(\frac{W}{m.K})$	27.5
$M(kg)$	0.085
$Q_{cell}(A.h)$	3

Table 1 Physical Properties of the Battery [13]

Moreover, the electrical resistance of the battery is dependent on SOC and the average volumetric temperature of the battery. In previous studies, it was noted that this resistance weakly depended on SOC [14]. The electrical resistance of the battery, therefore, in terms of its average volumetric temperature, was obtained [15] quantitatively from Equation (2). From Figure (2), it can be noted that the resistance is relatively constant at around (6 mΩ) within the operational temperature range of batteries in electric vehicles. Subsequently, for purposes of this study, it can be assumed that the electrical resistance of the battery is constant with a value of (6 mΩ). The current (I) is flowing through the battery. The notable point is that the current depends on the C-rate of the battery discharge, which is represented by Equation (3) [16]. The C-rate is the rate at which the charging and discharging processes occur for the battery within a time frame of one hour.

$$R_i(m\Omega) = -0.0001T_{avg}{}^3 + 0.0134T_{avg}{}^2 - 0.5345T_{avg} + 12.407 \quad (2)$$

$$I(A) = Q_{cell} \times C - rate \quad (3)$$

The current flow is induced at the initial temperature of 298.15 (K) with a constant Reynolds number of 100 that flows on one side of the enclosure, passes over the battery, and flows out from the other side, as evident from Figure (1). The Reynolds number is defined as:

$$\mathrm{Re}_D = \frac{\rho V D}{\mu} \quad (4)$$

Where ρ ($\frac{kg}{m^3}$) is density of fluid, V ($\frac{m}{s}$) is inlet velocity of coolant, and μ ($\frac{W}{m.k}$) demonstrates fluid dynamic viscosity. The thermophysical properties of coolant are calculated in ambient temperature as reference temperature.

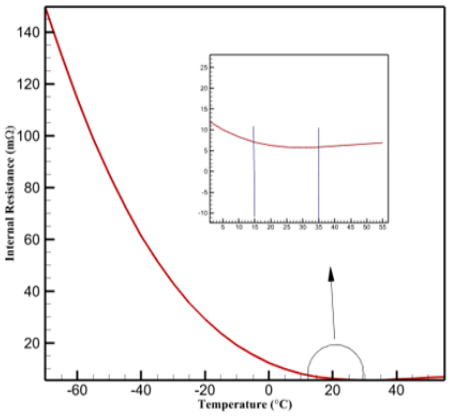

Fig.2 Battery Electrical Resistance Change with Temperature

From literature reviews [17], it is found that the formation of Karman vortex street (vortex shedding) is close to 48; Due to side walls, ceiling and bottom of the battery chamber, the transition is not Reynolds number driven alone, but geometry induced (confinement + wake interaction). Thus, the (SST k-ω) turbulent model was chosen for this simulation. The computational grid utilized in this simulation is structured and has 75880 cells, as evident from Figure (3), with a constant (Y+) value of 0.3 << 1 being maintained for the entire simulation.

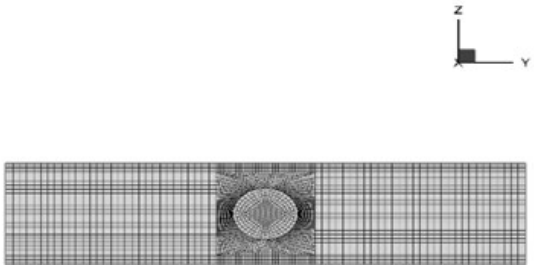

Fig.3 Top view of structural grid

It must be mentioned that the side walls, ceiling, and bottom of the enclosure have the thermal boundary conditions as insulated, and the side surface of the battery is coupled. The hydraulic boundary conditions at the inlet and outlet of the domain are specified as a constant velocity and $P = P_{atm}$, respectively. For convergence criteria, three monitors are defined: the velocity vector of the flow at a specific point, the coolant mass flow rate, and the inlet pressure along with a residual cutoff of E-06. Moreover, the solver settings include an initial time step of 10 (s), a Courant number of 1, and the SIMPLE pressure-velocity coupling method. The simulations have been carried out at a 4C discharge rate for the battery, as this rate imposes a significant loading on the battery and can also be taken as a conservative condition. As a result of this, it can be concluded from Equation (1), Equation (3) and Table (1) that the estimated power generation inside the battery is about 1.03 (W). The volume fractions of the nanoparticles were taken at three different values, i.e., 0, 0.02, and 0.04.

The thermophysical properties of the nanofluid were calculated according to equations (5) to (9), as outlined in [18]. It is noteworthy

that the properties of the base fluid (mineral oil) were assumed to be constant, corresponding to those at ambient temperature, since from Figure (8) it is clear that the temperature variation along the battery chamber is below 1.5 ℃ and according to literature [19], the thermophysical properties of oil are almost independent of temperature over this range. As a result, the nanofluid thermophysical properties, which are crucial for calculating Reynolds number, are calculated corresponding to ambient temperature. Moreover, by varying the volume fraction of nanoparticle, inlet velocity is manually adjusted to keep the Reynolds number equal to 100 for all cases. The properties of the nanoparticles and the base fluid were obtained from reference [19] and are detailed in Table (2).

$$\rho_f = (1-\varphi)\rho_b + \varphi\rho_p \quad (5)$$

Where φ is the volume fraction of Al2O3, ρ_p is the density of Al2O3 and ρ_b is the density of pure mineral oil.

Specific Heat Capacity:

$$C_{pf} = \frac{\left[(1-\varphi)\rho_b C_{pb} + \varphi\rho_p C_{pp}\right]}{\rho_f} \quad (۶)$$

Where C_{pp} is the specific heat capacity of Al2O3 and C_{pb} is the specific heat capacity of pure mineral oil.

Thermal Conductivity:

$$k_f = 0.25\left[(3\varphi-1)k_p + (2-3\varphi)k_b + \sqrt{\Delta}\right] \quad (۷)$$

Where k_p is the thermal conductivity of Al2O3 and k_b is the thermal conductivity of pure mineral oil.

Also:

$$\Delta = \left[(3\varphi-1)k_p + (2-3\varphi)k_b\right]^2 + 8k_p k_b \quad (۸)$$

Viscosity:

$$\mu_f = \mu_b(123\varphi^2 + 7.3\varphi + 1) \quad (9)$$

Where μ_b is the viscosity of pure mineral oil.

Name	Physical Properties	Value
Pure Mineral Oil	$C_p\ (\frac{J}{kg.K})$	1940.04
	$\rho\ (\frac{kg}{m^3})$	867
	$k(\frac{W}{m.K})$	0.133
	$\mu(Pa.s)$	0.0197
Al_2O_3	$C_p\ (\frac{J}{kg.K})$	765
	$\rho\ (\frac{kg}{m^3})$	3970
	$k(\frac{W}{m.K})$	40

Table 2 Physical Properties of Pure Mineral Oil and Al2O3 [1]

The flow is assumed to be turbulent due to Re > 48 and forementioned deduction. Ansys solves the Navier-Stokes equation on the conservation of mass, momentum, and energy, with the specified parameters and boundary conditions.

The governing equations are as follows.

Mass conversion :

$$\frac{\partial\rho_f}{\partial t} + \nabla\bullet(\rho_f\vec{V}) = 0 \quad (۱۰)$$

Where $\vec{V}$ demonstrates the velocity vector of fluid flow, regarding to incompressible coolant, it reduces to:

$$\nabla\bullet(\vec{V}) = 0 \quad (۱۱)$$

Momentum Conservation:

$$\frac{\partial(\rho_f\vec{V})}{\partial t} + \nabla\bullet(\rho_f\vec{V}\vec{V}) = -\nabla p + \nabla\bullet(\tau) + \rho_f\vec{g} \quad (۱۲)$$

Where $\vec{V}$ stands for velocity vector, p indicates static pressure of the working fluid and, τ is Stokes stress tensor.

Energy Conversion:

$$\frac{\partial(\rho_f h)}{\partial t} + \nabla\bullet(\rho_f h\vec{V}) = \nabla\bullet(k\nabla T) \quad (۱۳)$$

Where $\vec{V}$ is velocity vector, k stands for heat conduction coefficient of the working fluid and h is enthalpy of the fluid flow.

3- Results and Discussion

3-1 Mesh Independence

To investigate grid independence, three different structured meshes were employed, as outlined in Table (3). As observed in this table, the number of grid cells approximately doubles at each step. As observed in Figure (4), the average surface temperature of the battery was selected as the evaluation parameter. It is noted that the value of this parameter in Grid 2, which consists of 75880 cells, is approximately equivalent to that of the finer grid. Therefore, this grid configuration will be used for subsequent calculations in this study. It is worth mentioning that this analysis was conducted for a nanoparticle volume fraction of 0.04.

Table 3 Grids Detail

Grid number	Number of cells
1	39400
2	75880
3	145310

3-2 Validation

To verify the present calculation setup, Seider-Tate correlation [20] is validated for a quasi-channel flow that oil flows through a gap between four batteries quadrants, in which each of them is a quarter of an 18650 cylindrical Li-ion battery, along batteries' axis; While these batteries quadrants are tangent with their side cell. In the forementioned study, oil enters the gap with temperature of 20 ℃ and its thermophysical properties varies by temperature according to equations which are mentioned in the article. Moreover, each battery has a constant heat generation rate of 3 (W) and the flow regime is assumed to be laminar. Furthermore, the inlet temperature is assumed to be the reference temperature. Boundary conditions are shown in Figure (5).

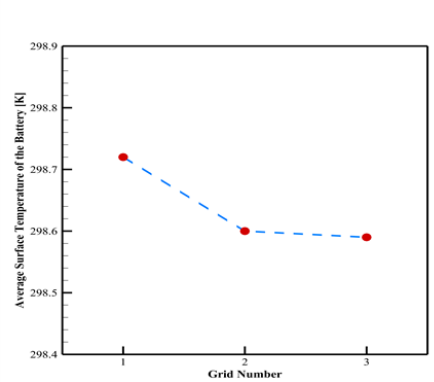

Fig.4 Mesh Sensitivity Analysis

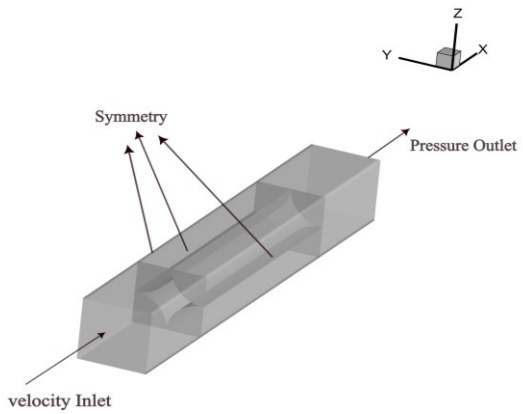

Fig.5 Validation setup

The Nusselt number of the fluid flow is chose as the evaluation parameter. Findings reveal a perfect alignment between simulation and empirical results. It is noteworthy that the error between data is below 5% in all points. As a result of this, the present numerical setup is valid and trusted.

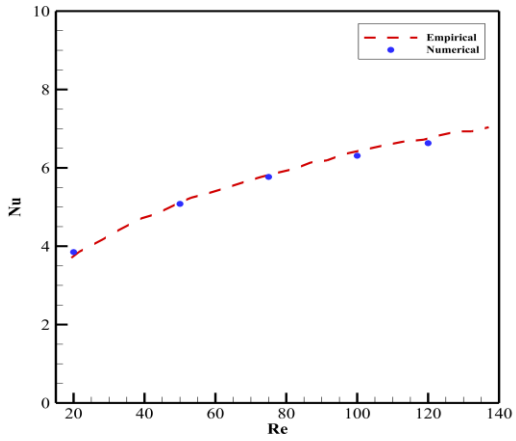

Fig. 6 Validation Results

3-3 Effect of volume fraction of the nanoparticle on heat transfer

To evaluate the variations in heat transfer within the thermal management system, the average convective heat transfer coefficient of the nanofluid and the average Nusselt number of the flow were utilized. Initially, energy conservation within the battery compartment was mentioned for a volume fraction of 0.02 as a representative case. Subsequently, the convective heat transfer coefficient of the nanofluid was calculated by defining the effective heat transfer surface and the reference temperature difference. Finally, the Nusselt number of the flow was compared across different volume fractions. It should be noted that, in this study, the film temperature was employed as the reference temperature. Additionally, to measure the average temperature values at the outlet of the domain and on the battery surface, the mass-weighted temperature and the area-weighted temperature were used, respectively.

Energy Balance inside the Battery considering constant current:

$$\dot{Q}_{store}[W] = \dot{Q}_{gen} - \dot{Q}_{loss} \quad (14)$$

Energy Conservation within the fluid domain:

$$\dot{Q}_{loss}[W] = \dot{m} C_{pf} \Delta T \quad (۱۵)$$

For the case under investigation with a volume fraction of 0.02, the values of the average temperature difference between the inlet and outlet, the specific heat capacity of the nanofluid, and the mass flow rate of the nanofluid were obtained as 0.001824 (K), 1839.5958 (J/kg·K), and 0.3076 (kg/s), respectively. Therefore:

$$\dot{Q}_{loss} = 1.032[W] \quad (۱۶)$$

On the other hand, by integrating over the effective heat transfer surface of the battery during the solution process, the total heat transfer rate, after reaching a steady state, was calculated to be 1.033 watts. Therefore:

$$\dot{Q}_{loss} = \int_{A_{effective}} \dot{Q} dA \quad (۱۷)$$

Effective surface of the heat transfer [21]

$$A_{effective} = \pi D h = 0.00539(m^2) \quad (۱۸)$$

Average heat transfer coefficient:

$$\overline{h}\left(\frac{W}{m^2.K}\right) = \frac{\dot{Q}_{loss}}{A_{effective} \times \Delta T_{ref}} \quad (۱۹)$$

Where:

$$\Delta T_{ref} = \overline{T}_{s,battery} - T_{film} \quad (20)$$

Also:

$$T_{film}(K) = \frac{1}{2}(\overline{T}_{s,battery} + T_{inlet}) \quad (۲۱)$$

Average Nusselt number of the fluid flow is calculated according to

$$\overline{Nu} = \overline{h}\frac{D}{k_f} \quad (22)$$

The variations in key parameters, including the average Nusselt number, the average convective heat transfer coefficient, and the pressure drop within the battery chamber, can be observed as the nanoparticle volume fraction changes from 0 to 0.04 at a constant inlet Reynolds number of 100, as presented in Table (4). Furthermore, the temperature, velocity, and pressure contours for the case with a volume fraction of 0.04 are provided below. Also, the variation of mean temperature of the battery surface over time is mentioned below, as Figure (11) illustrates.

Parameter	$Re_D = 100$			%(Δ)
	$\varphi = 0$	$\varphi = 0.02$	$\varphi = 0.04$	
$\overline{Nu}$	140.0952	151.7652	167.1778	19.33
$\overline{h}\left(\frac{W}{m^2.K}\right)$	709.2822	768.3653	846.3974	19.33
$\lvert\Delta P\rvert(pa)$	19.9584	26.6089	38.6709	93.75

Table ۴ Results

As the nanoparticle volume fraction increases from 0 to 0.04 at a constant inlet Reynolds number of 100, the heat transfer capability of the working fluid increases by approximately 20%.

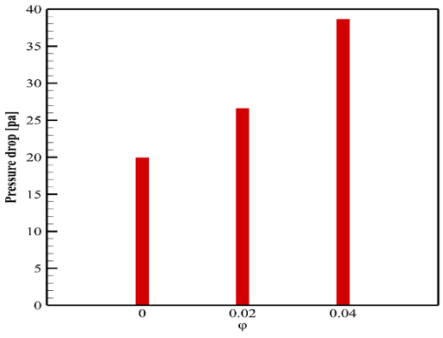

Fig.7 Pressure Drop in Battery Chamber

As it is clear, heat transfer enhancement is accompanied by a significant increase in pressure drop within the battery chamber, which approximately doubles under the same conditions.

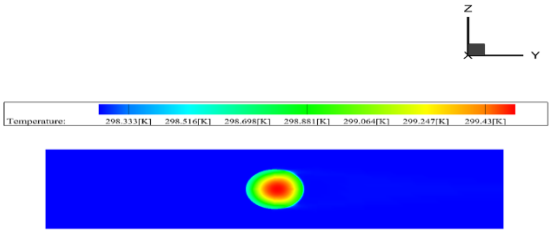

Fig.8 Contour of Temperature

This contour shows the heat diffusion inside the solid domain, which has been generated in the centerline and scatters inside the domain in radial direction.

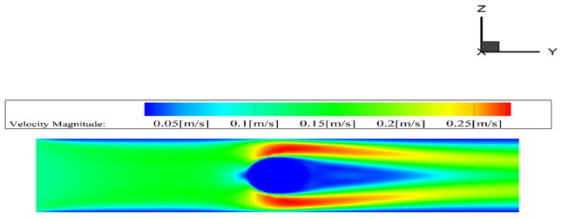

Fig.9 Contour of Velocity

This contour shows the maximum velocity, which has occurred between the battery and side walls, and also the formation of Von Karman vortex street behind the battery.

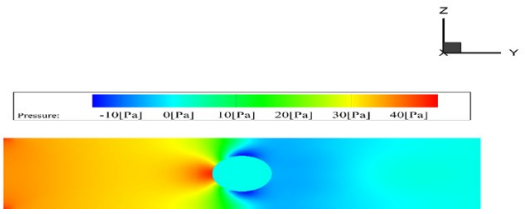

Fig.10 Contour of Pressure

This contour illustrates the pressure difference between upstream and downstream of the battery. Since drag force is achievable by integrating over battery surface, it is noteworthy that this force must be considered in module design. Additionally, this contour demonstrates the pressure drop between inlet and outlet of the fluid domain. Since hydraulic power is directly related to pressure drop and as it is well known that designing a battery thermal management system has always been a trade-off between costs and benefits, which are here appear in the form of pumping power and heat transfer enhancement, as a result, conducting a thermo-economic analysis is essential.

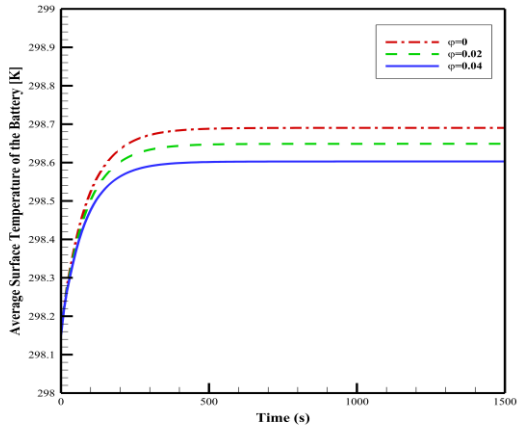

Fig.11 Variation of Mean Temperature of Battery Surface

This graph illustrates the variation in the mean surface temperature of the battery as a function of nanoparticle volume fraction. The addition of nanoparticles reduces the surface temperature of the battery and enhances heat transfer performance. Although the battery surface temperature remains within an acceptable range without additives, reducing the Reynolds number—potentially to lower pumping power requirements—increases the importance of using nanoparticles to maintain effective thermal management.

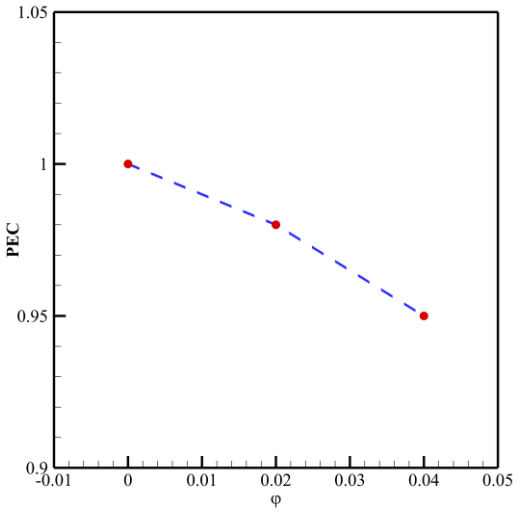

Fig. 12 Performance Efficiency Coefficient of nanofluid

3-4 Performance analysis

To investigate the effect of adding nanoparticles on the cooling performance of the battery chamber, Performance Efficiency Coefficient (PEC) is used. In present study, PEC is calculated based on pressure drop ratio [22]:

$$PEC = (h_{nf} / h_{oil}) / (\Delta P_{nf} / \Delta P_{oil}) \quad (23)$$

The result for different volume fractions is depicted in Figure (12). It is observable that by increasing the volume fraction of nanoparticles, PEC decreases, in which means that in this case heat

transfer enhancement cannot rectify the increase of pressure drop. This could be caused by different reasons such as limited heat transfer effective area, low Reynolds number, and harsh confinement. It should be noted that it does not mean that nanofluid is useless, but in present geometry with aforementioned Reynolds number, using nanofluid is not ideal in terms of thermohydraulic.

4- Conclusion

This study numerically evaluated the thermal performance of an alumina–oil nanofluid for cooling a lithium iron phosphate battery. The simulations demonstrated that incorporating nanoparticles into the base oil significantly enhances convective heat transfer characteristics. An increase in nanoparticle volume fraction up to 4% resulted in nearly a 20% improvement in the heat transfer coefficient. Although such thermal enhancement contributes to better temperature regulation, which is critical for maintaining battery safety and durability, it costs a significant increase in pressure drop along the battery chamber, which must be rectified by hydraulic pump that ultimately results in a slight decrease in performance efficiency of nanofluid.

Artificial Intelligence Statement:

During the preparation of this manuscript, the authors used ChatGPT solely to improve the grammar and language quality of the text. Following the use of this tool, the authors carefully reviewed and, where necessary, edited the content. The authors accept full responsibility for the content of the published manuscript.

Author Contributions:

Alireza Izanlou: Conceptualization, Methodology, Software, Investigation, Formal Analysis, Validation, Visualization, Writing-original draft.

Mohammad Hatami: Conceptualization, Methodology, Supervision, Writing - review & editing.

Ethics Approval:

The scientific content of this article is the result of the authors' research and has not been published in any Iranian or international journal.

Conflict of Interest:

The authors declare that there is no conflict of interest in preparing this paper.

References

[1] S. Al-Hallaj and J. R. Selman, "Thermal modeling of secondary lithium batteries for electric vehicle/hybrid electric vehicle applications." *Power Sources,* vol. 110, Aug. 2002, doi: 10.1016/S0378-7753(02)00196-9

[2] C. Aswin Karthik, P. Kalita, X. Cui, and X. Peng, "Thermal management for prevention of failures of lithium ion battery packs in electric vehicles: A review and critical future aspects," *Energy Storage*, vol. 2, no. 3, Jun. 2020, doi: 10.1002/est2.137.

[3] O. Kalkan, A. Celen, and K. Bakirci, "Experimental and numerical investigation of the LiFePO4 battery cooling by natural convection," *J Energy Storage*, vol. 40, Aug. 2021, doi: 10.1016/j.est.2021.102796.

[4] C. C. Cheng, P. C. Chang, H. C. Li, and F. I. Hsu, "Design of a single-phase immersion cooling system through experimental and numerical analysis," *Int J Heat Mass Transf*, vol. 160, Oct. 2020, doi: 10.1016/j.ijheatmasstransfer.2020.120203.

[5] Y. Zhou, Z. Wang, Z. Xie, and Y. Wang, "Parametric Investigation on the Performance of a Battery Thermal Management System with Immersion Cooling," *Energies (Basel)*, vol. 15, no. 7, Apr. 2022, doi: 10.3390/en15072554.

[6] M. Suresh Patil, J. H. Seo, and M. Y. Lee, "A novel dielectric fluid immersion cooling technology for Li-ion battery thermal management," *Energy Convers Manag*, vol. 229, Feb. 2021, doi: 10.1016/j.enconman.2020.113715.

[7] M. Rabiei, A. Gharehghani, and A. M. Andwari, "Enhancement of battery thermal management system using a novel structure of hybrid liquid cold plate," *Appl Therm Eng*, vol. 232, p. 121051, Sep. 2023, doi: 10.1016/j.applthermaleng.2023.121051.

[8] Z. Zou, J. Xie, Y. Luo, G. Zhang, and X. Yang, "Numerical study on a novel thermal management system coupling immersion cooling with cooling tubes for power battery modules," *J Energy Storage*, vol. 83, Apr. 2024, doi: 10.1016/j.est.2024.110634.

[9] S. Ahmad, Y. Liu, S. A. Khan, S. W. A. Shah, and X. Huang, "Modeling liquid immersion-cooling battery thermal management system and optimization via machine learning," *International Communications in Heat and Mass Transfer*, vol. 158, Nov. 2024, doi: 10.1016/j.icheatmasstransfer.2024.107835.

[10] H. Dai, C. Yang, F. Zhang, G. Liao, B. Zhang, and J. E, "Transient heat dissipation performance investigation on the battery thermal management system based on S-CO2 immersion cooling," *Energy*, vol. 318, Mar. 2025, doi: 10.1016/j.energy.2025.134656.

[11] V. G. Choudhari, D. A. S. Dhoble, and T. M. Sathe, "A review on effect of heat generation and various thermal management systems for lithium ion battery used for electric vehicle," Dec. 01, 2020, *Elsevier Ltd*. doi: 10.1016/j.est.2020.101729.

[12] S. Mazyar and H. Moghaddam, "Designing battery thermal management systems(BTMS) for cylindrical Lithium-ion battery modules using CFD."

[13] Dipl.-I. U. C. Huber, "Phase Change Material in Battery Thermal Management Applications An assessment of efficiency and safety."

[14] C. Park, A. K. Jaura, and C. Mesa, "Dynamic Thermal Model of Li-Ion Battery for Predictive Behavior in Hybrid and Fuel Cell Vehicles Reprinted From: Hybrid Vehicle and Energy Storage Technologies (SP-1789) Future Transportation Technology Conference," 2003.

[15] R. Mahamud and C. Park, "Reciprocating air flow for Li-ion battery thermal management to improve temperature uniformity," *J Power Sources*, vol. 196, no. 13, pp. 5685–5696, Jul. 2011, doi: 10.1016/j.jpowsour.2011.02.076.

[16] S. Panchal, "Experimental Investigation and Modeling of Lithium-ion Battery Cells and Packs for Electric Vehicles."

[17] M. M. Zdravkovich, "Conceptual Overview of Laminar and Turbulent Flows Past Smooth and Rough Circular Cylinders." *Journal of Wind Engineering and Industrial Aerodynamics,* vol. 33, no 1-2, pp. 53-62, Mar. 1990, doi: 10.1016/0167-6105(90)90020-D

[18] M. V. Bozorg, M. Hossein Doranehgard, K. Hong, and Q. Xiong, "CFD study of heat transfer and fluid flow in a parabolic trough solar receiver with internal annular porous structure and synthetic oil–Al2O3 nanofluid," *Renew Energy*, vol. 145, pp. 2598–2614, Jan. 2020, doi: 10.1016/j.renene.2019.08.042.

[19] Niazmand A, Prajwal M, Satyam S, Pardeep S, Pratik B, and Dereje A, "Numerical Analysis Of Oil Immersion Cooling Of a Server Using Mineral Oil And Al2O3 Nanofluid," *ASME* , 2020.

[20] Camilleri R, Sawani M, "Prediction of the Heat Transfer Coefficient in Direct Oil Cooling of Lithium-Ion Batteries," *IEEE 2018.*

[21] R. D. Jilte and R. Kumar, "Numerical investigation on cooling performance of Li-ion battery thermal management system at high galvanostatic discharge," *Engineering Science and Technology, an International Journal*, vol. 21, no. 5, pp. 957–969, Oct. 2018, doi: 10.1016/j.jestch.2018.07.015.

[22] Kong M, Lee S, "Performance Evaluation of Al2O3 Nanofluid as an Enhanced Heat Transfer Fluid," *Advances in Mechanical Engineering,* vol. 12, Aug. 2020, doi: 10.1177/1687814020952277